(p,γ) rates of ^{92}Mo, ^{94}Mo, ^{95}Mo, ^{98}Mo: Towards an experimentally founded database for p-process studies

T. Sauter and F. Käppeler
Forschungszentrum Karlsruhe, Institut für Kernphysik, Postfach 3640, D-76021 Karlsruhe, Germany
(Received 14 February 1997)

The proton capture cross sections of the stable molybdenum isotopes 92, 94, 95, and 98 have been measured by means of the activation method in the proton energy range between 1.5 and 3 MeV. Thin layers of natural molybdenum were irradiated at the Karlsruhe 3.75 MV Van de Graaff accelerator with proton beams of 20–55 μA. The activity induced by (p,γ) reactions was measured with a calibrated HPGe detector. In this way, six cross sections for populating ground states and isomers in four different Tc isotopes could be determined simultaneously. The systematic uncertainties of this method are typically 4%. The fact that the resulting cross sections are 2–4 times larger than recent statistical model predictions illustrates the need of experimental data for the yet unexplored field of (p,γ) reactions in the mass region beyond $A=90$. The present results are important for a quantitative discussion of the production of the abundant p nuclei ^{92}Mo, ^{94}Mo, ^{96}Ru, and ^{98}Ru during SN Ia explosions. They represent also a first step in establishing parameter systematics that allow for more reliable model extrapolations into the region of unstable nuclei of relevance for the p process in SN II. [S0556-2813(97)05006-1]

PACS number(s): 25.40.Lw, 26.30.+k, 27.60.+j, 97.10.Tk

I. INTRODUCTION

The 32 stable isotopes on the proton-rich side of the chart of nuclides between ^{74}Se and ^{196}Hg, which are 10 to 100 times less abundant than the s- and r-process nuclei, are assumed to originate from the modification of an s or r seed in the p process. The presently favored sites for the p process are the explosively burning O/Ne layers in supernovas (SN) of type II, where temperatures of $T_9 \sim 2$–3 ($T_9 = 10^9$) are maintained for about 1 s at densities of $\sim 10^6$ g cm^{-3}. Under these conditions, proton-rich nuclei are produced by a sequence of (γ,n) reactions. When this sequence is halted after five to ten steps by the increasing neutron separation energies, the further reaction flow is dominated by the (γ,p) and (γ,α) channels. As the temperature decreases during the explosion, the reaction path moves back to the region of stable nuclei. This scenario involves about 1000 nuclei and 10 000 reactions. Similar conditions apply for supernovas of type Ia with the important difference that a significant amount of free protons are released in the carbon burning zones.

Compared to the SN scenarios, previously proposed sites for a pure (p,γ) origin of the p nuclei appear less promising, because novas are not efficient enough to account for the observed abundances [1], and Thorne-Żytkow objects [2] are still rather speculative.

In view of the huge number of reactions required for p-process studies it is hard to believe that experimental data are almost completely missing. Apart from a single (p,γ) cross section for ^{90}Zr [3], two (α,γ) values for ^{70}Ge and ^{144}Sm [4,5], as well as a few (n,γ) rates for some stable p nuclei [6], p-process calculations had to rely completely on theoretical data.

Despite the uncertain nuclear physics, p-process models for SN II and for SN Ia are capable of reproducing the p nuclei within a factor of 3 [7–9]. However, both scenarios do have problems in describing the light p-nuclei with $A<100$ correctly. Since the p process in SN II is dominated by photodisintegrations from heavy seeds, this model does not account for the relatively large abundances of ^{92}Mo, ^{94}Mo, ^{96}Ru, and ^{98}Ru (see Fig. 1). In SN Ia models, this deficiency is compensated by the fact that protons are released in carbon burning and captured by the abundant neutron magic isotopes with $N=82$, thus contributing the missing p-process components of Mo and Ru. However, this effect is also felt by the lighter p nuclei ^{74}Se, ^{78}Kr, and ^{84}Sr which are, therefore, systematically overproduced.

These difficulties may suggest that some fraction of the critical Mo and Ru isotopes could have been synthesized in other processes. These include mainly neutrino-induced reactions in current r-process scenarios [10] as well as the rp process associated with explosive hydrogen burning in x-ray bursters as discussed by Schatz *et al.* [11].

In any case, a more rigorous treatment of these open questions requires definitely a considerable improvement of the underlying nuclear physics data. Consequently, the present interest in the (p,γ) cross sections of the molybdenum isotopes is motivated by two aspects: To test the quality of existing model calculations in the stability valley around $A=90$ which are important for describing the (p,γ) sequence along the magic neutron number $N=50$ (SN Ia), and to establish a consistent parameter systematics for improving the calculated reaction rates of the entire p-process network (SN Ia, SN II). Naturally, the second aim requires many more experimental data over a larger mass range. Though the present work can only be considered as a first step in this direction, it introduces the activation technique as an efficient way to collect a fair number of data in a reasonable time and at reasonable costs.

In Sec. II, the experimental technique and the sample preparation are outlined, followed by the description of the irradiations (Sec. III) and data analysis (Sec. IV). The results

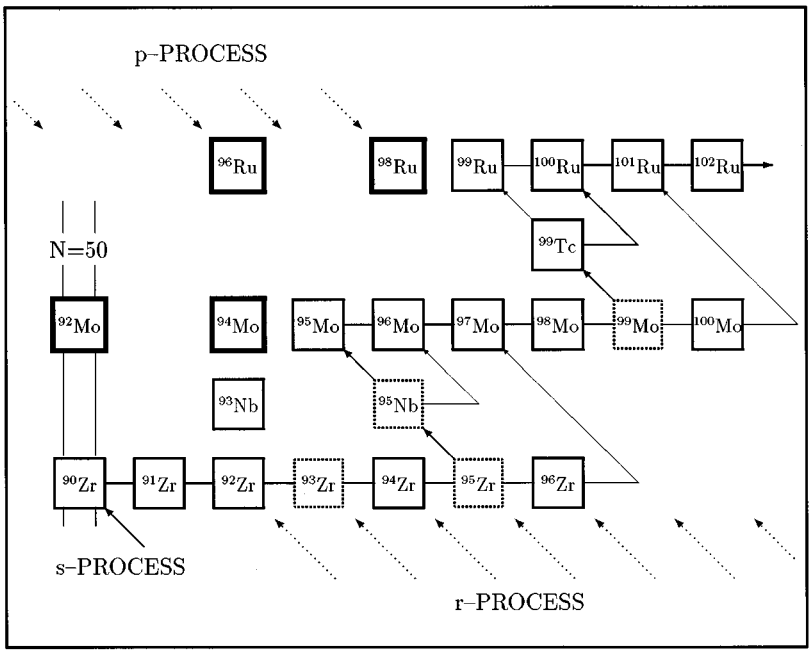

FIG. 1. The isotopes in the mass region between Zr and Ru. The main nucleosynthesis mechanisms in this mass region, the *s* and *r* process, are both bypassing the *p* nuclei ^{92}Mo, ^{94}Mo, ^{96}Ru, and ^{98}Ru.

are presented directly as (p,γ) cross sections as well as in the form of astrophysical *S* factors and reaction rates (Sec. VI).

II. EXPERIMENTAL TECHNIQUE

Though very common in applied research, the activation technique has recently been used in the field of astrophysics only for (n,γ) work in the context of *s*-process studies [12]. For charged particle capture reactions, the direct observation of the prompt capture γ rays became the standard technique instead, thanks to the excellent energy resolution of Ge detectors. This advantage is, however, no longer relevant for $A>60$ due to the increasing complexity of the capture γ-ray spectra, a difficulty that was encountered, for example, in the only previous (p,γ) study of relevance for the *p* process [3]. Hence, the merits of the activation technique appear increasingly attractive for this type of experiment: it is fairly simple, it exhibits good sensitivity, and it is selective for specific reactions via the decay of the product nuclei. This latter aspect allows us not only to use samples of natural composition, but offers the possibility to determine several cross sections in a single measurement. There is also the option for determining partial cross sections to long-lived isomers with half-lives longer than the *p*-process time scale of a few seconds. In such cases, the ground state and isomer should be considered in the reaction network as separate species. All these aspects are illustrated in the following sections.

A. Investigated reactions

Proton irradiation of natural Mo yields observable activities from the decay of the reaction products ^{93m,g}Tc, ^{95m,g}Tc, ^{96}Tc, and ^{99m}Tc. This means that the (p,γ) reactions on ^{92}Mo, ^{94}Mo, ^{95}Mo, and ^{98}Mo can be investigated simultaneously in a single activation measurement. Capture reactions on the remaining Mo isotopes lead to Tc products which are either too short- or too long-lived for a reliable detection.

The decay of the activated Tc nuclei can be followed via the emitted γ radiation. The half-lives, the relative intensities per decay, and the information on cascading transitions were taken from the latest evaluations in Nuclear Data Sheets. All decay parameters used in this work are summarized in Table I.

B. Target preparation and definition

The targets consisted of metallic Mo layers sputtered onto polished aluminum disks of 1 mm thickness and 35 mm diameter. Aluminum was chosen for the backings in view of its good heat conductivity, and since proton captures are leading to ^{28}Si without producing any disturbing activity. Furthermore, its low atomic number is an important prerequisite for determining the target thickness via Rutherford backscattering as described below.

The Mo layers of 10 mm diameter were prepared by sputtering in an Ar atmosphere of 40 Pa [13]. This technique which is based on a controlled discharge allows us to produce chemically clean and uniform layers independent of the high melting point of Mo (2617 °C). The sputter yield can be adjusted by tuning the Ar pressure and/or the electric field of the discharge, resulting in a well-defined deposition rate.

In total, 50 Mo targets were prepared for the present experiment with typical sputter times of 10–15 min. The layer thickness was chosen between 1200 and 5000 Å corresponding to proton energy losses of 10 to 40 keV in the investigated energy range. This represents a compromise between the necessity to achieve an adequate activity in the irradiations and to determine the cross sections with reasonable energy resolution.

The target thickness was determined in two ways, by Rutherford backscattering (RBS) and by x-ray fluorescence

TABLE I. Decay properties of the product nuclei.

Product nucleus	Reference		Half-life	Gamma-ray energy, (keV)	Relative intensity per decay (%)
^{93}Tc	[22]	Ground state	2.75±0.05 h	1362.9	56.5±0.8
				1477.1	6.95±0.35
				1520.3	20.51±0.54
	[23]	Isomer	43.5±1.0 min	391.8	57.6±0.9
^{95}Tc	[24]	Ground state	20.0±0.1 h	765.8	93.8±0.3
				947.7	1.95±0.02
				1073.7	3.74±0.04
	[24]	Isomer	61±2 d	204.1	63.2±0.8
				582.1	29.9±0.4
				835.6	26.6±0.4
^{96}Tc	[25]	Ground state	4.28±0.7 d	778.2	99.76±0.01
				812.5	82.00±0.35
				849.9	97.57±0.38
^{99}Tc	[26]	Isomer	6.01±0.01 h	140.5	89.06±0.24

analysis (XRF). The RBS technique is based on the elastic backscattering of a light projectile from a heavy target. The energy difference of protons with energy E_0 scattered from different target nuclei M_i is

$$\Delta E \simeq E_0(4-\delta^2)\frac{M_1}{M_2^2}\Delta M, \tag{1}$$

where $\delta = 30$ deg is the difference between π and the scattering angle θ that follows from the geometry of the present setup. The relevant features of this technique are illustrated in Fig. 2 which compares the RBS spectra of a very thin Ta reference sample with the spectrum of a 2400-Å thick Mo layer. Both spectra were taken with a proton energy of 1.0 MeV and a beam current of 2 μA. These conditions were further on adopted for all RBS analyses. Obviously, the proton energy loss is larger for Mo (and much larger for Al) than for the heavier Ta nuclei. At the same time, the Mo peak is broader than that of the very thin Ta sample due to the proton energy losses in the comparably thick Mo layer. These losses are also responsible for the shift of the aluminum edge. The spectrum in the lower part of Fig. 2, which is representative for most of the investigated targets, indicates a homogeneous composition of the Mo layer. However, a few exceptions were showing symmetric structures on top of the backscatter peaks due to channeling effects, evidence that these layers had developed a polycrystalline structure.

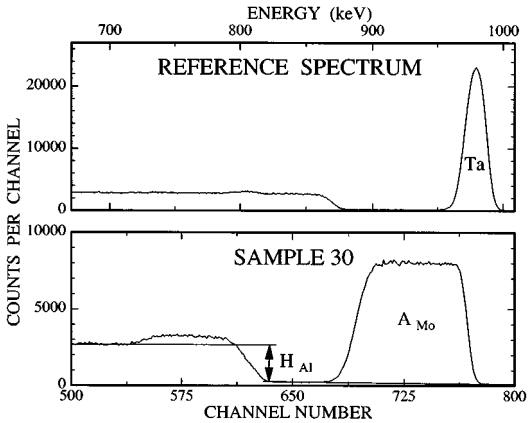

FIG. 2. RBS spectra from a very thin tantalum reference sample (top) and from one of the molybdenum samples (bottom). The molybdenum layer exhibits a significant oxygen content which shows up on top of the contribution from the aluminum backing.

For the interpretation of the RBS spectra with respect to target thickness the area A under the backscatter peaks was analyzed rather than the width, since the latter suffered significant broadening due to the oxygen content of the Mo layers.

The number of backscattered projectiles is

$$A = \frac{d\sigma}{d\Omega}\Omega Q N, \tag{2}$$

where $d\sigma/d\Omega$ denotes the differential scattering cross section, Ω is the solid angle between target and detector, Q is the number of incident projectiles, and N is the number density of the target.

The solid angle can be determined from the height of the aluminum edge. For normal incidence one gets

$$H_{\mathrm{Al}} = \frac{\sigma_{\mathrm{Al}}\Omega Q \xi}{\zeta_{\mathrm{Al}}} \tag{3}$$

where the energy bin per channel ξ can be obtained from the spectrum of the Ta reference sample, and ζ is the effective stopping cross section [14]. Combination of Eqs. (2) and (3) yields the number density of the Mo layers

TABLE II. Activation schemes and sample characteristics.

Activations				Samples		
Run	Proton energy (keV)	Beam current (μA)	Accumulated charge (mC)	Sample number	Proton energy loss [a] (keV)	Number density [b] (10^{17} at/cm^2)
1	1500	39	420	50	40	31.4±1.0
2	1599	25	270	45	30	24.4±0.8
3	1700	30	330	15	18	15.4±0.5
4	1801	47	510	49	33	28.8±0.9
5	1840	47	610	47	27	24.1±0.7
6	1901	56	600	46	27	24.3±0.8
7	1950	48	520	42	26	23.9±0.8
8	2000	50	540	44	25	23.4±0.7
9	2050	44	480	41	24	21.7±0.7
10	2099	53	570	43	23	21.7±0.7
11	2099	35	380	35	23	21.6±0.7
12	2151	56	610	38	20	18.2±0.6
13	2189	53	570	37	19	18.6±0.6
14	2250	50	540	36	19	18.3±0.6
15	2300	52	560	34	19	19.4±0.6
16	2350	47	590	33	15	15.1±0.4
17	2400	44	470	29	16	16.4±0.5
18	2448	45	490	28	17	17.1±0.5
19	2475	13	150	32	17	17.4±0.5
20	2500	41	440	27	13	13.8±0.4
21	2550	44	480	25	13	13.7±0.4
22	2600	43	460	24	15	16.1±0.5
23	2649	46	580	23	10	11.3±0.3
24	2680	12	130	9	13	15.0±0.5
25	2700	42	530	22	11	12.1±0.4
26	2750	35	380	11	12	13.5±0.4
27	2800	30	320	8	9	10.3±0.3
28	2850	40	430	6	9	10.4±0.3
29	2900	28	250	13	9	10.4±0.3
30	2950	19	200	14	11	13.3±0.4
31	3003	16	170	7	9	7.8±0.2

[a]See text.
[b]Average of XRF and RBS results.

$$N_{\mathrm{Mo}}=\frac{A_{\mathrm{Mo}}\sigma_{\mathrm{Al}}\xi}{H_{\mathrm{Al}}\sigma_{\mathrm{Mo}}\zeta_{\mathrm{Al}}}. \tag{4}$$

The RBS analyses, which were carried out with the code RUMP [15], exhibit typical uncertainties of ± 5%.

The second determination of the target thickness via XRF made use of a crystal spectrometer (Siemens SRS 3000) operated with a LiF (100) crystal and a rhodium anode, so that all elements up to Mo could be detected. At lower energies, the fluorescence yield was measured with a gas counter, and a NaI scintillator was used for the higher energies.

The spectrometer was calibrated by means of five reference samples consisting of well defined amounts of Mo, Cu, and Fe. The Cu and Fe components were added to simulate possible contaminations of the Mo layers in the sputtering process. The reference samples were prepared from standard solutions and had the same diameter as the actual Mo samples.

The XRF results showed indeed contaminations up to 10 μg Cu and 28 μg Fe. Based on the RBS spectra it could be excluded, however, that these contaminations occurred in the Mo layers. This was supported by the fact that the contaminations were not correlated with the Mo mass. This means that the detected Cu and Fe components were not imported by the sputtering process but are likely due to impurities in the target backings, well compatible with the specified Al quality of 99.5%.

The main uncertainties of the XRF results originate from the preparation of the reference samples ($\sim$ 3.5 %) and from counting statistics ($\leqslant$ 1%). Within the specified uncertainties, both methods are in perfect agreement. The finally

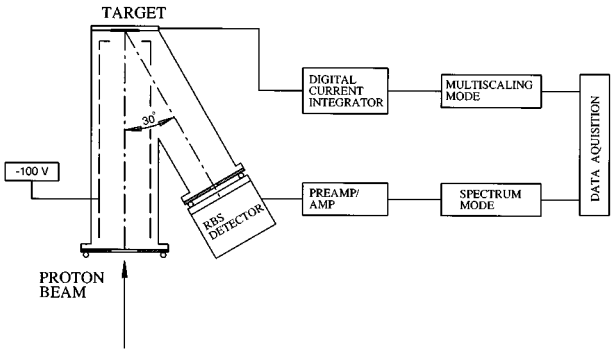

FIG. 3. Schematic setup for the activation at the accelerator. The proton beam current and the spectrum of backscattered protons were continuously monitored for later correction of the decay of activated nuclei during the irradiation and for sample degradation.

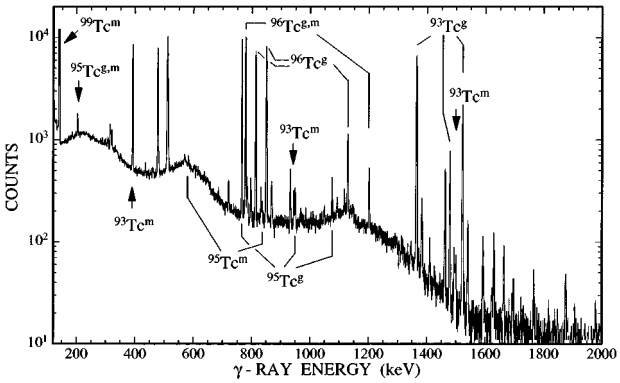

FIG. 4. Gamma-ray spectrum measured after activation of a molybdenum sample. The γ lines used in the data analysis are indicated for the various isotopes.

adopted number densities are the weighted average of the RBS and XRF results and carry a systematic uncertainty of 3% (Table II).

C. Experimental setup

The experimental setup used for the proton irradiations at the Karlsruhe 3.75 MV Van de Graaff is sketched in Fig. 3. The proton beam was well defined by two slit pairs on both sides of the analyzing magnet and a water-cooled diaphragm with 8 mm diameter mounted 30 mm in front of the target. The opening of this diaphragm being 2 mm narrower than the target diameter ensured that the sample was always hit by the full proton beam. For achieving a uniform distribution of the thermal load and a homogeneous illumination of the sample the beam was wobbled across the diaphragm by two deflection magnets situated downstream of the second slit pair.

The design of the activation chamber considered a number of relevant features. Electrically insulated from all other components of the beam line it acted as a Faraday cup for the complete collection of the accumulated charge. The emission of secondary electrons was suppressed by a copper liner that was put on negative potential. This liner was cooled with liquid nitrogen in order to trap organic vapors.

The targets were water-cooled from the rear and could be operated with beam currents of up to 100 μA, twice as much as was actually used in the present experiment. The RBS detector was kept in place also during the actual activations with a reduced entrance aperture of 0.5 mm diameter and served as a monitor for the target performance during the activation.

Figure 3 illustrates also the data acquisition during the activations. The collected charge was digitized and recorded in multiscaling mode with a resolution of 1 min/channel. In this way, variations of the proton beam current with time can be properly considered in the correction for the fraction of activated nuclei, which decay already during the irradiation.

III. MEASUREMENTS

A. Activations

The experiment was carried out in energy steps of 50 keV, spanning the range from 1.5 to 3.0 MeV that is most relevant for p-process studies. The proton beam energy was calibrated via the 2625 and 2326 keV resonances of the ^{34}S$(p,\gamma)^{35}$Cl reaction as well as the neutron threshold of the ^{7}Li(p,n) reaction at 1881 keV. The uncertainties of this calibration were comparable to the 0.1 % energy spread of the proton beam and, hence, much smaller than the target thickness. In order to achieve sufficient counting statistics the target thickness was chosen to correspond to proton energy losses of 25 keV around 2 MeV proton energy. The irradiations were carried out with very stable beam currents of typically 45 μA and lasted between 3 and 4 h.

To ensure that the targets suffered no losses or unacceptable degradations during the activations, RBS spectra were taken in regular intervals. In these measurements, the low-

TABLE III. Compilation of systematic uncertainties (%).

	^{92}Mo$(p,\gamma)^{93}$Tc		^{94}Mo$(p,\gamma)^{95}$Tc		^{95}Mo$(p,\gamma)^{96}$Tc	^{98}Mo$(p,\gamma)^{99m}$Tc
Source of uncertainty	g.s.	Isomer	g.s.	Isomer		
Half-life	2.0	2.3	0.7	4.7	2.3	0.2
γ intensity per decay, I_γ	1.4	1.6	0.3	1.3	0.01	0.3
Isomer decay to g.s., η	1.1	1.4	0.1	0.1	0.5	
Cascade corrections	0.4		0.5	1.0	1.4	
Efficiency of γ detector, ϵ_γ				1.5		
Target thickness				3.0		
Proton-beam current				1.0		

TABLE IV. Measured (p,γ) cross sections and S factors of ^{92}Mo.

Energy bin (keV)	Cross section (μb)		S factor (10^9 keV b)	
	Ground state	Total [a]	Ground state	Total [a]
1480±20	0.080±0.021	0.139±0.022	80±29	139±40
1585±15	0.258±0.023	0.455±0.027	87±16	154±26
1695±6	0.146±0.186	0.206±0.186	18±20	25±23
1785±17	0.764±0.059	1.50±0.07	44±8	86±13
1836±14	0.961±0.063	2.09±0.08	37±5	79±10
1888±14	1.80±0.10	3.40±0.12	46±6	87±10
1937±13	3.33±0.18	6.17±0.22	59±7	110±12
1988±13	1.67±0.11	3.40±0.13	20.8±2.4	42.3±4.5
2038±12	5.08±0.33	10.9±0.4	45.0±4.8	96±9
2088±12	4.15±0.26	8.64±0.33	26.5±2.7	55.3±5.0
2088±12	3.91±0.28	8.69±0.34	25.0±2.7	55.5±5.0
2141±10	3.70±0.19	6.30±0.22	16.9±1.4	28.8±2.2
2180±10	13.4±0.7	24.5±0.9	48.4±4.0	88.9±6.5
2241±10	3.64±0.20	6.74±0.23	9.2±7.3	17.0±1.2
2290±10	9.40±0.53	18.5±0.6	17.9±1.5	35.4±2.4
2343±8	5.72±0.39	14.1±0.5	8.2±0.7	20.2±1.2
2392±8	17.8±1.5	51.6±2.1	19.8±1.9	57.1±3.5
2440±8	17.0±1.0	34.3±1.4	14.7±1.1	29.7±1.8
2467±8	26.9±1.7	54.0±2.2	20.4±1.6	40.8±2.5
2494±7	11.6±0.8	27.9±1.0	7.6±0.6	18.5±0.9
2544±7	16.3±0.9	34.2±1.2	8.5±0.6	17.8±0.8
2592±8	22.7±1.2	38.7±1.5	9.4±0.6	16.1±0.9
2644±5	16.1±1.0	31.2±1.2	5.3±0.3	10.3±0.5
2673±7	24.2±1.7	55.7±2.2	7.0±0.5	16.1±0.8
2695±6	15.7±1.1	31.5±1.5	4.1±0.3	8.3±0.5
2744±6	34.6±2.2	65.1±2.7	7.4±0.5	13.9±0.6
2795±5	43.5±2.5	81.1±3.3	7.5±0.5	14.0±0.6
2846±5	56.8±4.4	110±6	8.0±0.6	15.4±0.9
2895±5	35.5±1.7	53.3±2.3	4.1±0.2	6.2±0.3
2945±5	63.5±3.1	109±4	6.1±0.3	10.4±0.4
2998±5	57.6±3.4	116±4	4.5±0.3	9.1±0.4

[a]Sum of partial (p,γ) cross sections to ground state and isomer, absolute uncertainties added in quadrature.

energy part of the spectrum was suppressed by a thin Al foil in front of the solid-state detector. The subsequent RBS spectra showed very good agreement throughout the activations so that Mo losses from the targets could be excluded. Blister formation in the Al backings by the implanted hydrogen could be tolerated. Only two targets, where the blisters broke open, had to be exempted from further analysis. As an additional check, the reduction of the beam current by a factor three in a few activations showed no statistically significant effect on the deduced (p,γ) cross sections, thus confirming that the targets were not deteriorated by the beam.

In total, 31 targets were activated in the present measurement. The parameters characterizing the Mo samples and the activations are summarized in Table II.

B. γ counting

The induced activities were counted off-line with a 265 cm^3 HPGe detector which was mounted in a $23\times23\times30$ cm thick lead shield with an internal 1.5 mm thick Cu absorber for suppression of the Pb x rays. The remaining background in the energy interval $200 \leqslant E_\gamma \leqslant 3400$ keV was 4 s^{-1}. All γ-ray spectra were analyzed with the SAMPO code [16].

The counting geometry was chosen as a compromise between high efficiency and acceptable cascade corrections. These corrections are required if a γ ray is registered coincident with another one from the same cascade or with a related, characteristic x ray. Since this effect increases rapidly with ϵ_γ, the targets were placed in a thin-walled plexiglass holder at 50 mm distance from the detector so that γ counting was always performed in a well defined position.

In this geometry, the detector was calibrated with a set of monoenergetic sources (^{139}Ce, ^{51}Cr, ^{85}Sr, ^{137}Cs, ^{54}Mn, and ^{65}Zn with lines at 165, 320, 514, 662, 834, and 1115 keV, respectively) as well as with sources emitting γ cascades (^{57}Co: 122/136 keV, ^{113}Sn: 255/392 keV, and ^{88}Y: 898/1836/2734 keV). Additionally, an ^{241}Am source (60 keV) was used for determining the cascade correction for coincident x rays. The cascade corrections were calculated with the code CASC [17] by due consideration of the counting geometry, and using the complete spectroscopic information from

TABLE V. Measured (p,γ) cross sections and S factors of ^{94}Mo.

Energy bin (keV)	Cross section (μb)		S factor (10^9 keV b)	
	Ground state	Total [a]	Ground state	Total [a]
1480±20	0.036±0.008	[b]	35.5±12	[b]
1586±15	0.11±0.03	[b]	38.0±12	[b]
1695±6	0.34±0.04	[b]	41.7±5	[b]
1784±17	0.66±0.04	1.9±0.6	37.6±6	112.0±39
1836±14	0.59±0.03	[b]	22.5±3	[b]
1888±14	1.67±0.07	3.55±0.58	42.6±5	91.0±18
1938±14	1.85±0.08	[b]	32.7±3.7	[b]
1988±13	2.44±0.10	7.33±0.87	30.4±3.2	91.2±13.9
2038±12	3.07±0.13	11.5±1.5	27.1±2.6	101.5±16.2
2088±12	2.79±0.11	8.14±1.25	17.8±1.6	52.1±9.1
2088±12	2.83±0.13	[b]	18.1±1.5	[b]
2141±10	4.91±0.23	11.8±1.4	22.5±1.8	53.8±7.4
2179±10	7.55±0.28	21.2±1.5	27.4±2.0	76.7±7.3
2241±10	8.80±0.45	26.7±1.9	22.2±1.7	67.3±6.2
2290±10	12.6±0.6	33.7±1.7	24.1±1.9	64.4±5.0
2343±8	16.2±0.6	39.0±2.0	23.3±1.3	56.0±3.8
2392±8	19.2±0.8	47.5±3.3	21.2±1.3	52.2±4.4
2440±8	23.6±1.3	60.3±3.8	20.4±1.4	52.2±4.0
2467±9	30.5±1.6	80.9±5.8	23.0±1.6	61.1±5.1
2494±7	41.3±3.0	104±5	27.3±2..2	68.9±4.4

[a] Sum of partial (p,γ) cross sections to ground state and isomer, absolute uncertainties added in quadrature.
[b] Yield too small for meaningful analysis.

the latest compilations (see Table I for the respective references). The corrections could be verified via the spectra from sources with cascading transitions, thus confirming an overall systematic uncertainty of 1.5% for ϵ_γ and a 10% uncertainty for the calculated cascade corrections.

During the activity measurements, which lasted for 8 to 12 h, γ-ray spectra were stored every 30 min. In this way, the induced activities could be followed with respect to their half-lives. This was particularly important for separating the decay components of the various Tc isotopes. In all activations, pile-up corrections were negligibly small.

IV. DATA ANALYSIS

Proton captures in most Mo isotopes populate the ground state and isomer in the respective Tc products. In the analysis of the subsequent decay chains the additional feeding of the ground state by internal transitions from the isomer has to be considered. The population of isomer, $M(t)$, and ground state, $G(t)$, is described by

$$\frac{dM(t)}{dt} = -\lambda_m M(t) + \sigma_m \Phi(t) N_0, \tag{5}$$

$$\frac{dG(t)}{dt} = -\lambda_g G(t) + \eta\lambda_m M(t) + \sigma_g \Phi(t) N_0, \tag{6}$$

where σ_g, σ_m are the partial cross sections to ground state and isomer, $\Phi(t)$ denotes the proton flux, and η is the decay branch from the isomer to the ground state.

For constant proton flux these equations can be solved analytically, but the more realistic time-dependent case requires numerical integration. Using the recorded multiscaling spectrum of the proton current and assuming that the proton current is constant during the time intervals Δt one obtains for the number of activated nuclei after an irradiation time t_b:

$$M(t_b) = \sigma_m N_0 \frac{1-e^{-\lambda_m \Delta t}}{\lambda_m} \sum_{i=1}^{n} \Phi_i e^{-(n-i)\lambda_m \Delta t}, \tag{7}$$

$$\begin{aligned} G(t_b) = {} & \sigma_g N_0 \frac{1-e^{-\lambda_g \Delta t}}{\lambda_g} \sum_{i=1}^{n} \Phi_i e^{-(n-i)\lambda_g \Delta t} \\ & + \eta\sigma_m N_0 \left(\frac{1-e^{-\lambda_g \Delta t}}{\lambda_g} \right. \\ & \left. - \frac{e^{-\lambda_m \Delta t} - e^{-\lambda_g \Delta t}}{\lambda_g - \lambda_m} \right) \sum_{i=1}^{n} \Phi_i e^{-(n-i)\lambda_g \Delta t} \\ & + \sum_{i=1}^{n} \frac{\lambda_m}{\lambda_g - \lambda_m} (e^{-\lambda_m \Delta t} - e^{-\lambda_g \Delta t}) \eta M_{i-1} e^{-(n-i)\lambda_g \Delta t}. \end{aligned} \tag{8}$$

The number of decays during the subsequent counting time t_m is

$$N_M = M(t_b) e^{-\lambda_m t_w} (1 - e^{-\lambda_m t_m}), \tag{9}$$

TABLE VI. Measured (p,γ) cross sections and S factors of ^{95}Mo and ^{98}Mo.

Energy bin (keV)	Cross sections (μb)		S factors (10^9 keV b)	
	^{95}Mo$(p,\gamma)^{96}$Tc	^{98}Mo$(p,\gamma)^{99m}$Tc	^{95}Mo$(p,\gamma)^{96}$Tc	^{98}Mo$(p,\gamma)^{99m}$Tc
1480±20	[a]	0.054±0.002	[a]	54.1±13.1
1586±15	[a]	0.144±0.006	[a]	48.9±7.8
1695±5	0.58±0.06	0.367±0.014	71.4±8.1	44.8±2.8
1785±17	1.51±0.07	0.885±0.033	86.6±13.5	50.7±7.6
1836±14	2.27±0.17	1.18±0.04	86.0±12.2	44.8±5.5
1888±14	3.55±0.14	1.64±0.06	91.0±10.8	42.0±4.8
1938±14	4.73±0.19	2.56±0.10	83.6±9.5	45.2±5.0
1988±13	7.29±0.37	3.47±0.13	90.8±9.8	43.3±4.4
2038±12	8.48±0.33	4.51±0.17	75.1±7.0	40.0±3.4
2089±12	13.3±0.5	6.22±0.22	84.8±7.0	39.7±3.4
2089±12	13.9±0.6	6.77±0.24	88.0±8.3	43.0±3.7
2141±10	17.9±0.7	8.84±0.33	82.0±6.5	40.4±3.1
2179±10	27.8±1.0	11.5±0.4	101.0±7.4	41.8±3.0
2241±10	31.4±1.2	14.4±0.5	79.2±5.5	36.4±2.5
2290±10	42.5±1.6	20.7±0.7	81.3±5.6	39.5±2.7
2343±8	53.9±1.9	25.8±0.9	77.2±4.5	37.0±2.1
2392±8	70.7±2.6	30.5±1.1	78.3±4.5	33.8±1.9
2440±9	87.3±3.3	40.9±1.5	75.6±4.5	35.4±2.0
2467±8	106±4	47.9±1.8	80.4±4.7	36.2±2.1
2494±7	108±4	50.4±1.8	71.4±3.6	33.4±1.7
2544±7	122±4	65.3±2.2	63.7±3.1	34.1±1.6
2593±8	110±4	52.6±1.9	45.7±2.5	21.9±1.1
2644±5	105±4	29.7±1.0	34.5±1.5	9.8±0.4
2673±7	132±5	31.7±1.1	38.3±1.9	9.2±0.4
2695±6	131±5	20.5±0.7	34.5±1.6	5.4±0.2
2744±6	155±6	13.2±0.5	33.1±1.6	2.8±0.1
2795±5	137±5	11.1±0.4	23.7±1.0	1.91±0.08
2845±5	156±5	10.9±0.4	22.0±0.9	1.53±0.06
2895±5	128±5	8.89±0.32	14.8±0.6	1.00±0.04
2945±6	147±6	9.87±0.36	14.1±0.6	0.95±0.04
2998±5	146±5	9.64±0.35	11.4±0.5	0.76±0.03

[a]Yield too small for meaningful analysis.

$$N_G = G(t_b)(1-e^{-\lambda_g t_m})e^{-\lambda_g t_w} + \frac{\eta\lambda_m\lambda_g M(t_b)}{\lambda_m-\lambda_g}\left(\frac{e^{-\lambda_g t_w}}{\lambda_g}(1-e^{-\lambda_g t_m}) - \frac{e^{-\lambda_m t_w}}{\lambda_m}(1-e^{-\lambda_m t_m})\right), \quad (10)$$

where t_w, t_m stand for the waiting time between activation and counting and for the counting time, respectively.

The net counts, C_γ, for each of the peaks in Fig. 4 can be expressed as

$$C_\gamma = \frac{NK_\gamma\epsilon_\gamma I_\gamma}{C_p}, \quad (11)$$

where N denotes the total number of activated nuclei at the end of irradiation, ϵ_γ is the efficiency of the HPGe detector, I_γ is the relative γ-ray intensity per decay, and K_γ is the correction for γ-ray self-absorption in the target, which was always negligibly small.

The systematic uncertainties are summarized in Table III. The uncertainties of the respective half-lives, which contribute according to Eqs. (9) and (10) via the decay rates λ_i, can be important. The other decay parameters, I_γ and η, are rather well known and, therefore, less relevant for the overall uncertainty.

The uncertainties related to γ counting due to the detector efficiency and the cascade corrections have been discussed before. This holds also for the thickness of the Mo layers, which account for the largest contribution to the systematic uncertainty. The uncertainty of the proton-beam determination was found to be ±1 % due to the design of the target chamber. Possible current losses through the cooling water were checked with a battery and could be neglected. Below about 2 MeV proton energy, the total uncertainties are dominated by counting statistics.

The cross sections were determined independently for each of the lines listed in Table I, and these results were combined to the weighted means that are presented in Tables IV–VI. The uncertainties of these results range typically around 4% and were obtained by error propagation. In evalu-

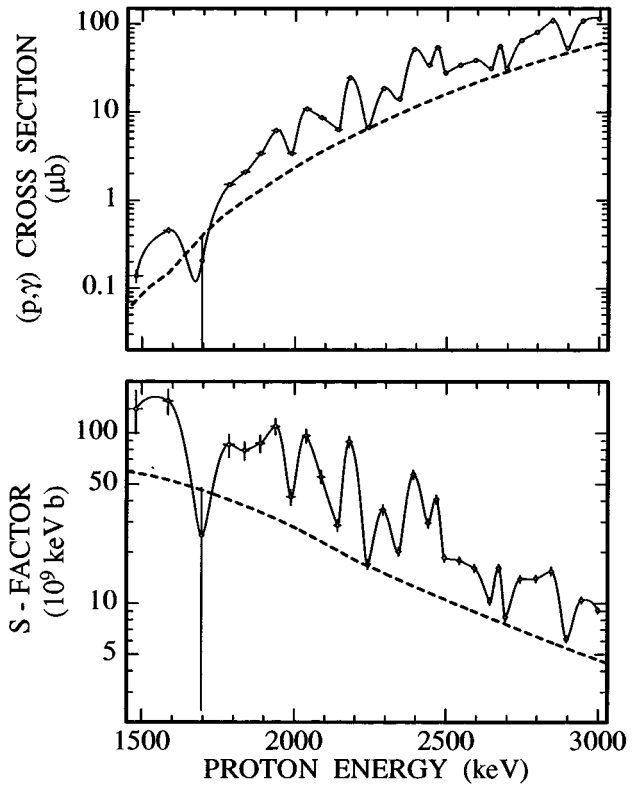

FIG. 5. The (p,γ) cross section of ^{92}Mo (top) and the corresponding S factor (bottom) compared to a statistical model calculation [18] (dashed line).

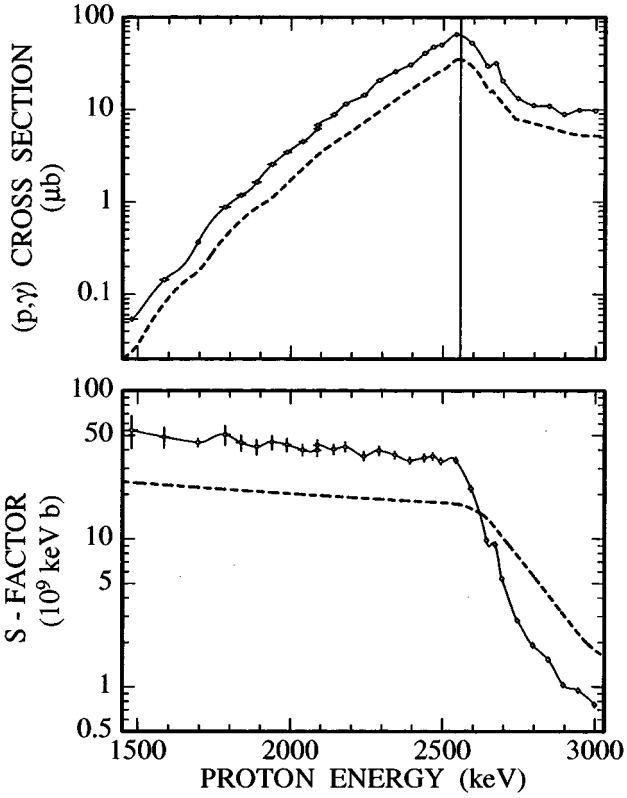

FIG. 6. The partial (p,γ) cross section of ^{98}Mo to the isomer in ^{99}Tc (top) and the corresponding S factor (bottom) compared to a statistical model calculation [18] (dashed line). The (p,n) threshold refers to the third excited state in ^{98}Tc at 73 keV.

ating the uncertainty of the total reaction cross sections for ^{92}Mo and ^{94}Mo from the measured partial cross sections the covariance between isomer and ground state was always found to be very small. Therefore, the uncertainty of the total cross section was conservatively estimated by quadratic summation of the uncertainties obtained for the partial cross sections.

V. RESULTS AND DISCUSSION

The experimental (p,γ) cross sections and the corresponding astrophysical S factors are summarized in Tables IV–VI. The following discussion of the various reactions deals with the peculiarities of the respective decay schemes, the problem of partial cross sections for populating ground states and isomers, and the competition by other reaction channels.

A. ^{92}Mo$(p,\gamma)^{93}$Tc

Proton capture populates the ground state ($t_{1/2}$=2.75 h) and the isomer ($t_{1/2}$=43.5 min) with about equal probability. The decay of ^{93}Tc feeds only levels in ^{93}Mo which decay directly to the ground state. Therefore, no cascade corrections were required in this case except a 4% summing-out correction due to possible coincidences with x rays from the electron capture (EC) branch of the decay. The decay of the isomer was followed via the internal transition.

The sum of the two partial cross sections is plotted in Fig. 5. The large uncertainty of the point at 1695 keV results from the small target thickness in this activation. In this case, the activity of the ground-state decay was too small for direct observation so that only an upper limit could be derived. The fluctuations in the cross section reflect the small level density of the neutron magic nucleus ^{92}Mo.

For comparison, recently calculated (p,γ) cross sections [18] are included in Fig. 5 by a dashed line. These data were calculated with the Hauser-Feshbach code SMOKER [19] and

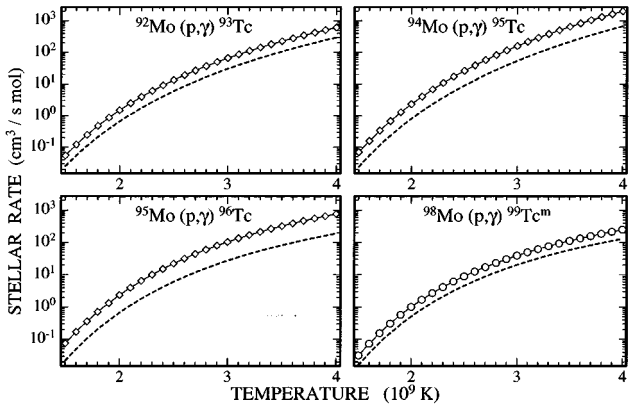

FIG. 7. The total rates of the (p,γ) reactions on ^{92}Mo, ^{94}Mo, and ^{95}Mo (diamonds) and the partial rate to the isomer ^{99m}Tc compared to a statistical model calculation [18] (dashed line).

refer also to the respective targets in the ground state. While the cross section shape is in very good agreement, the absolute magnitude is clearly underestimated by the calculation.

Such calculations were performed for all reactions investigated in this work and will be mentioned also in connection with Figs. 6 and 7. This comparison is restricted to one set of calculations to simply illustrate the possible differences. At a later stage, when more experimental data became available, a more thorough discussion must include all theoretical input data that are used in p-process studies.

B. ^{94}Mo$(p,\gamma)^{95}$Tc

Also for this reaction, the partial cross sections for populating ground-state ($t_{1/2}$=20 h) and isomer ($t_{1/2}$=61 d) could be derived. While the ground-state decay could again be followed by direct transitions, cascade corrections of 10–12% were required for the isomer decay. Though the partial cross section to the isomer is about 50% larger than the one to the ground state, this component could not always be detected at lower proton energies because of the long half-life of the isomer.

The ^{94}Mo cross section exhibits a much smoother shape and is significantly larger than that of ^{92}Mo, reflecting the higher level density of the target nucleus. The data for this reaction are limited to proton energies below 2.5 MeV where the threshold of the ^{95}Mo$(p,n)^{95}$Tc reaction is reached which leads to the same reaction product.

C. ^{95}Mo$(p,\gamma)^{96}$Tc

In this case a meaningful evaluation of the partial cross section to the isomer ^{95m}Mo with $t_{1/2}$=51.5 min was not possible because of the very uncertain γ intensities in the weak β^+/EC decay of this isomer. Qualitatively, however, the data indicate that the partial cross section to the isomer dominates the total (p,γ) rate of ^{95}Mo by far (see Table VII).

In view of these problems, only the total cross section was deduced by observing a waiting time between activation and γ counting of at least four half-lives. For the following ground-state decay ($t_{1/2}$=4.28 d) cascade corrections of 14% had to be considered.

This cross section was found to vary smoothly with proton energy until a clear change in slope at 2.5 MeV marks the position of the (p,n) threshold.

D. ^{98}Mo$(p,\gamma)^{99}$Tc

The ground state of ^{99}Tc is too long-lived ($t_{1/2}$=2.1 10^5 yr) for the activation technique to be applied. Therefore, only the partial cross section to the 6 h isomer could be determined. The cross section (Fig. 6) shows a significant edge due to the competition by the (p,n) reaction, much stronger than predicted by the calculation. This edge is so pronounced that it is clearly incompatible with the (p,n) threshold for the ground state in ^{98}Tc at 2493 keV which is plausible in view of the large spin difference between ^{98}Mo and ^{98}Tc. Instead, the location of the edge shows that the (p,n) reaction involves the third excited state in ^{98}Tc at 73.3 keV. For this state, the present experiment is compatible with $J^\pi = 0^-$, 1^-, or 2^-, in agreement with the tentative assignment of $J^\pi = 2^-$ [20].

TABLE VII. Total (p,γ) rates for ^{92}Mo, ^{94}Mo, ^{95}Mo and the partial rate for ^{98}Mo$(p,\gamma)^{99m}$Tc.

Temperature (10^9 deg)	^{92}Mo	^{94}Mo	^{95}Mo	^{98}Mo$(p,\gamma)^{99m}$Tc
1.5	0.055	0.070	0.075	0.0316
1.6	0.121	0.159	0.171	0.0731
1.7	0.248	0.338	0.361	0.156
1.8	0.475	0.677	0.712	0.308
1.9	0.861	1.28	1.33	0.573
2.0	1.49	2.32	2.35	1.01
2.1	2.47	4.03	3.97	1.69
2.2	3.94	6.74	6.43	2.70
2.3	6.08	10.9	10.0	4.16
2.4	9.12	17.1	15.1	6.20
2.5	13.3	26.2	22.2	8.96
2.6	19.1	39.1	31.6	12.6
2.7	26.7	57.1	44.0	17.3
2.8	36.6	81.8	59.9	23.2
2.9	49.4	115	79.9	30.4
3.0	65.7	159	105	39.3
3.1	86.1	216	135	49.8
3.2	111	290	171	62.3
3.3	143	383	214	76.9
3.4	180	501	265	93.7
3.5	226	647	323	113
3.6	280	827	391	135
3.7	344	1050	468	159
3.8	420	1310	555	186
3.9	509	1630	653	216
4.0	612	2000	763	249

E. Reaction rates

The experimental (p,γ) cross sections were used to determine the stellar reaction rates

$$\langle \sigma v \rangle = \left(\frac{8}{\pi \mu} \right)^{1/2} \frac{N_A}{(kT)^{3/2}} \int_0^\infty \sigma(E) E \exp\left(-\frac{E}{kT} \right) dE, \tag{12}$$

where N_A is the Avogadro number. Outside the investigated energy range, the measured cross sections were complemented by the normalized calculated data. In Fig. 7 the stellar rates listed in Table VII are plotted versus temperature and compared to the theoretical values of Ref. [18]. In all cases, there is good agreement as far as the temperature dependence is concerned, but the absolute values for the total (p,γ) rates differ by factors of 2.2, 2.9, and 3.7 for the reactions ^{92}Mo$(p,\gamma)^{93}$Tc, ^{94}Mo$(p,\gamma)^{95}$Tc, and ^{95}Mo$(p,\gamma)^{96}$Tc, respectively. That these factors increase with neutron number may indicate a systematic trend in the Hauser-Feshbach parametrization.

For the easier use of these data in complex p-process networks, the curves in Fig. 7 have been fitted according to Woosley *et al.* [21]:

$$\langle \sigma v \rangle = T_9^{-2/3} \exp[A - (\tau / T_9^{1/3})(1 + B T_9 + C T_9^2 + D T_9^3)] \quad \text{cm}^3/\text{s mol}, \tag{13}$$

TABLE VIII. Fit parameters for the temperature dependence of the investigated (p,γ) rates.

Reaction	A	B	C	D
^{92}Mo$(p,\gamma)^{93m}$Tc	43.118	1.664×10^{-2}	8.548×10^{-3}	-1.106×10^{-3}
^{92}Mo$(p,\gamma)^{93g}$Tc	44.324	4.062×10^{-2}	2.654×10^{-3}	-5.722×10^{-4}
^{92}Mo$(p,\gamma)^{93}$Tc	44.457	2.953×10^{-2}	5.361×10^{-3}	-8.152×10^{-4}
^{94}Mo$(p,\gamma)^{95m}$Tc	43.823	3.172×10^{-2}	-1.134×10^{-3}	2.624×10^{-5}
^{94}Mo$(p,\gamma)^{95g}$Tc	43.019	2.771×10^{-2}	-8.947×10^{-4}	5.195×10^{-5}
^{94}Mo$(p,\gamma)^{95}$Tc	44.402	3.402×10^{-2}	-1.809×10^{-3}	9.740×10^{-5}
^{95}Mo$(p,\gamma)^{96}$Tc	42.681	-1.319×10^{-2}	1.374×10^{-2}	-1.204×10^{-3}
^{98}Mo$(p,\gamma)^{99m}$Tc	40.400	-4.859×10^{-2}	2.492×10^{-2}	-2.355×10^{-3}

where $\tau=4.2487(Z_1^2Z_2^2\mu)^{1/3}$. The respective parameters are summarized in Table VIII.

VI. SUMMARY

In this work the activation technique was shown to represent an efficient tool for the reliable determination of (p,γ) cross sections for p-process studies. Though mostly restricted to measurements on stable target nuclei, this method offers the possibility to establish an extended set of data for testing and normalizing the parameter systematics for Hauser-Feshbach extrapolations to the actual reaction network of the p process.

Despite its formal simplicity, measurements with the activation technique require great care in technical details if its full potential is to be exploited. Most crucial in this respect are the preparation and characterization of the targets, but also monitoring of the proton yield and of the target performance throughout the irradiations are important. The subsequent γ counting requires carefully calibrated detectors including the verification of count rate corrections due to cascade effects and/or the coincident observations of related x rays. If these precautions are considered, cross sections can be determined with uncertainties of a few % as was here demonstrated at the example of the Mo isotopes.

The present results may have an immediate impact on the p process in SN Ia, where proton captures on an existing seed may affect the abundances of the light p nuclei, in particular of the abundant species ^{92}Mo and ^{94}Mo. Beyond this aspect, they are intended as a first step towards a comprehensive experimental basis for increasingly quantitative p-process calculations.

ACKNOWLEDGMENTS

We thank A. Ernst, E. P. Knaetsch, D. Roller, and W. Seith for their help and support during the irradiations at the Van de Graaff accelerator as well as G. Rupp for his excellent technical assistance throughout the entire experiment. We are also indebted to many people from different departments of Forschungszentrum Karlsruhe, in particular to G. Linker and R. Fromknecht for their help with the RBS analyses and to D. Hentschel S. Fetzner for enabling the XRF measurements.

[1] D. Lambert, Astron. Astrophys. Rev. **3**, 201 (1992).
[2] G. Biehle, Astrophys. J. **380**, 167 (1991).
[3] C. Laird, D. Flynn, R. Hershberger, and F. Gabbard, Phys. Rev. C **35**, 1265 (1987).
[4] Z. Fülöp *et al.*, Z. Phys. A **355**, 203 (1996).
[5] E. Somorjai *et al.*, in *Nuclei in the Cosmos '96*, edited by M. Wiescher [Nucl. Phys. (to be published)].
[6] Z. Bao and F. Käppeler, At. Data Nucl. Data Tables **36**, 411 (1987).
[7] N. Prantzos, M. Hashimoto, M. Rayet, and M. Arnould, Astron. Astrophys. **238**, 455 (1990).
[8] W. Howard, B. Meyer, and S. Woosley, Astrophys. J. **373**, L5 (1991).
[9] M. Rayet *et al.*, Astron. Astrophys. **298**, 517 (1995).
[10] G. Fuller and B. Meyer, Astrophys. J. Suppl. Ser. **48**, 279 (1982).
[11] H. Schatz *et al.*, in *Nuclei in the Cosmos ' 96* [5].
[12] F. Käppeler, H. Beer, and K. Wisshak, Rep. Prog. Phys. **52**, 945 (1989).
[13] P. Townsend, J. Kelly, and N. Hartley, *Ion Implantation, Sputtering and their Applications* (Academic, New York, 1976), p. 111.
[14] J. F. Ziegler, in *Handbook of Stopping Cross-Sections for Energetic Ions in all Elements, Vol. 5*, edited by J. F. Ziegler (Pergamon, New York, 1980), p. 275.
[15] L. Doolittle, Nucl. Instrum. Methods Phys. Res. B **15**, 227 (1986).
[16] J. Routti and S. Prussin, Nucl. Instrum. Methods **72**, 125 (1969).
[17] S. Jaag, Technical report 51.01.01/P02B, Kernforschungszentrum Karlsruhe (unpublished).
[18] H. Schatz (private communication).
[19] J. Cowan, F.-K. Thielemann, and J. Truran, Phys. Rep. **208**, 267 (1991).

[20] B. Singh, Nucl. Data Sheets **67**, 693 (1992).
[21] S. Woosley, W. Fowler, J. Holmes, and B. Zimmerman, At. Data Nucl. Data Tables **22**, 371 (1978).
[22] H. Sievers, Nucl. Data Sheets **54**, 99 (1988).
[23] C. Baglin, Nucl. Data Sheets **70**, 1 (1993).
[24] T. Burrows, Nucl. Data Sheets **68**, 635 (1993).
[25] L. Peker, Nucl. Data Sheets **68**, 165 (1993).
[26] L. Peker, Nucl. Data Sheets **73**, 1 (1994).